The Astrophysical Journal, 611:517–527, 2004 August 10

DIVERSITY AND ORIGIN OF 2:1 ORBITAL RESONANCES IN EXTRASOLAR PLANETARY SYSTEMS

Man Hoi Lee
Department of Physics, University of California, Santa Barbara, CA 93106-9530; mhlee@europa.physics.ucsb.edu
Received 2004 January 16; accepted 2004 April 23

ABSTRACT

A diversity of 2:1 resonance configurations can be expected in extrasolar planetary systems, and their geometry can provide information about the origin of the resonances. Assembly during planet formation by the differential migration of planets due to planet-disk interaction is one scenario for the origin of mean-motion resonances in extrasolar planetary systems. The stable 2:1 resonance configurations that can be reached by differential migration of planets with constant masses and initially coplanar and nearly circular orbits are (1) antisymmetric configurations with the mean-motion resonance variables $\theta_1 = \lambda_1 - 2\lambda_2 + \varpi_1$ and $\theta_2 = \lambda_1 - 2\lambda_2 + \varpi_2$ (where λ_j and ϖ_j are the mean longitudes and the longitudes of periapse, respectively) librating about 0° and 180°, respectively (as in the Io-Europa pair), (2) symmetric configurations with both θ_1 and θ_2 librating about 0° (as in the GJ 876 system), and (3) asymmetric configurations with θ_1 and θ_2 librating about angles far from either 0° or 180°. There are, however, stable 2:1 resonance configurations with symmetric ($\theta_1 \approx \theta_2 \approx 0^\circ$), asymmetric, and antisymmetric ($\theta_1 \approx 180^\circ$ and $\theta_2 \approx 0^\circ$) librations that cannot be reached by differential migration of planets with constant masses and initially coplanar and nearly circular orbits. If real systems with these configurations are ever found, their origin would require (1) a change in the planetary mass ratio m_1/m_2 during migration, (2) a migration scenario involving inclination resonances, or (3) multiple-planet scattering in crowded planetary systems. We find that the asymmetric configurations with large e_2 and the $\theta_1 \approx 180^\circ$ and $\theta_2 \approx 0^\circ$ configurations have intersecting orbits and that the $\theta_1 \approx \theta_2 \approx 0^\circ$ configurations with $e_1 > 0.714$ have prograde periapse precessions.

Subject headings: celestial mechanics — planetary systems — planets and satellites: general

1. INTRODUCTION

Mean-motion resonances may be ubiquitous in extrasolar planetary systems. There are as many as three resonant pairs of planets in the 12 multiple-planet systems discovered to date. It is well established that the two planets about the star GJ 876 discovered by Marcy et al. (2001) are in 2:1 orbital resonance, with both lowest order, eccentricity-type mean-motion resonance variables,

$$\theta_1 = \lambda_1 - 2\lambda_2 + \varpi_1 \tag{1}$$

and

$$\theta_2 = \lambda_1 - 2\lambda_2 + \varpi_2 \tag{2}$$

(where $\lambda_{1,2}$ are the mean longitudes of the inner and outer planets, respectively, and $\varpi_{1,2}$ are the longitudes of periapse), librating about 0° (Laughlin & Chambers 2001; Rivera & Lissauer 2001; Lee & Peale 2002). The simultaneous librations of θ_1 and θ_2, and hence the secular apsidal resonance variable

$$\theta_3 = \varpi_1 - \varpi_2 = \theta_1 - \theta_2, \tag{3}$$

about 0° mean that the periapses are nearly aligned and that conjunctions of the planets occur when both planets are near periapse. The other two pairs of planets suspected to be in mean-motion resonances are the pair about HD 82943, in 2:1 resonance (Mayor et al. 2004), and the inner two planets about 55 Cnc, in 3:1 resonance (Marcy et al. 2002).

The symmetric geometry of the 2:1 resonances in the GJ 876 system was not expected, because the familiar 2:1 resonances between the Jovian satellites Io and Europa are antisymmetric, with θ_1 librating about 0° but θ_2 and θ_3 librating about 180° (a configuration that would persist in the absence of the Laplace resonance with Ganymede). In the Io-Europa case, the periapses are nearly antialigned, and conjunctions occur when Io is near periapse and Europa is near apoapse. Lee & Peale (2002) have shown that the differences in the resonance configurations are mainly due to the magnitudes of the orbital eccentricities involved (see also Beaugé & Michtchenko 2003). When the eccentricities are small, the Io-Europa configuration is expected from the resonant perturbation theory to the lowest order in the eccentricities. However, the eccentricities of the GJ 876 system are sufficiently large that there are large contributions from higher order terms, and stable simultaneous librations of θ_1 and θ_2 require $\theta_1 \approx \theta_2 \approx 0^\circ$ for a system with eccentricities and masses like those in GJ 876.

A scenario for the origin of mean-motion resonances in extrasolar planetary systems is that they were assembled during planet formation by the differential migration of planets due to gravitational interaction with the circumstellar disk from which the planets formed. A single giant planet (with a planet-to-star mass ratio greater than ~a few times 10^{-4}) can open an annular gap in the circumstellar gas disk about the planet's orbit. If a disk forms two giant planets that are not very far apart (with the ratio of the orbital semimajor axes $a_1/a_2 \sim 1/2$), the planets can also clear the disk material between them rather quickly (Bryden et al. 2000; Kley 2000; Kley et al. 2004). Disk material outside the outer planet exerts torques on the planet that are not opposed by disk material on the inside, and the outer planet migrates toward the star. Any disk material left on the inside of the inner planet exerts torques on the inner planet that push it away from the star. The

timescale on which the planets migrate is the disk viscous timescale, whose inverse is

$$\left|\frac{\dot{a}}{a}\right| \approx \frac{3\nu}{2a^2} = \frac{3}{2}\alpha\left(\frac{H}{a}\right)^2\Omega = 9.4\times10^{-5}\left(\frac{\alpha}{4\times10^{-3}}\right)\left(\frac{H/a}{0.05}\right)^2 P^{-1} \quad (4)$$

(Ward 1997), where $\dot{a} \equiv da/dt$, the kinematic viscosity ν is expressed using the Shakura-Sunyaev α-prescription ($\nu = \alpha H^2\Omega$), H is the scale height of the disk, and $\Omega = 2\pi/P$ and $P \approx 2\pi a^{3/2}/(Gm_0)^{1/2}$ are, respectively, the mean motion and period of an orbit of semimajor axis a. Although the depletion of the inner disk means that the inner planet may not move out very far, the condition of approaching orbits for capture into mean-motion resonances is established.

Lee & Peale (2002) have shown that the observed symmetric, 2:1 resonance configuration in the GJ 876 system can be easily established by the differential migration due to planet-disk interaction (see also Snellgrove et al. 2001). They have also found that the observed eccentricities of the GJ 876 system require either significant eccentricity damping from planet-disk interaction or resonance capture occurring just before nebula dispersal, because continued migration of the planets while locked in the 2:1 resonances can lead to rapid growth of the eccentricities if there is no eccentricity damping. As we see in § 4, there are other types of stable 2:1 resonance configurations with large eccentricities for a system with the inner-to-outer planet mass ratio, m_1/m_2, of the GJ 876 system, but these configurations are either unstable for planets as massive as those in GJ 876 or not reachable by differential migration of planets with constant masses and coplanar orbits.

As Lee & Peale (2002) pointed out, a practical way to investigate what stable resonance configurations are possible from continued migration of the planets after capture into 2:1 resonances is through numerical migration calculations without eccentricity damping. Either eccentricity damping or the termination of migration due to nebula dispersal would lead to a system being left somewhere along a sequence. They noted that asymmetric resonance configurations with θ_1 and θ_2 librating about angles other than 0° and 180° are possible for systems with m_1/m_2 different from that in GJ 876. Lee & Peale (2003a) have presented some results on the variety of stable 2:1 resonance configurations that can be reached by differential migration (see also Ferraz-Mello et al. 2003). Asymmetric librations were previously only known to exist for exterior resonances in the restricted three-body problem (e.g., Message 1958; Beaugé 1994; Malhotra 1999). Other recent works on 2:1 resonance configurations for two-planet systems include those by Beaugé et al. (2003), Hadjidemetriou & Psychoyos (2003), Ji et al. (2003), and Thommes & Lissauer (2003). With the exception of Thommes & Lissauer (2003), who examined the possibility of inclination resonances for non-coplanar orbits, all of the works mentioned in this paragraph have focused on systems with two planets on coplanar orbits.

In this paper we present the results of a series of direct numerical orbit integrations of planar two-planet systems designed to address the following questions: What are the possible planar 2:1 resonance configurations? Can they all be obtained by differential migration of planets? In § 2 we describe the numerical methods. In § 3 we present the stable 2:1 resonance configurations that can be reached by differential migration of planets with constant masses. The analysis in § 3 is an extension of those by Lee & Peale (2003a) and Ferraz-Mello et al. (2003). We consider configurations with $0.1 \le m_1/m_2 \le 10$ and an orbital eccentricity of the inner planet, e_1, up to 0.8 and provide a detailed analysis of properties such as the boundaries in m_1/m_2 for different types of evolution, the region in parameter space for configurations with intersecting orbits, and the region where the retrograde periapse precessions expected for orbits in 2:1 resonances are reversed to prograde. By using a combination of calculations in which m_1/m_2 is changed slowly and differential migration calculations, we show in § 4.1 that there are also symmetric and asymmetric 2:1 resonance configurations that cannot be reached by differential migration of planets with constant masses. In their studies of systems with masses similar to those in HD 82943, Ji et al. (2003) and Hadjidemetriou & Psychoyos (2003) have discovered antisymmetric 2:1 resonance configurations with $\theta_1 \approx 180^\circ$ and $\theta_2 \approx 0^\circ$. We show in § 4.2 that a sequence of this configuration with antialigned, intersecting orbits exists for all m_1/m_2 examined. In § 5 we summarize our results and describe several mechanisms by which the configurations found in § 4 can be reached.

2. NUMERICAL METHODS

We consider a system consisting of a central star of mass m_0, an inner planet of mass m_1, and an outer planet of mass m_2, with the planets on coplanar orbits. We refer to the planet with the smaller orbital semimajor axis as the inner planet, but it should be noted that some of the configurations studied below have intersecting orbits, and the outer planet can be closer to the star than the inner planet some of the time. In addition to the mutual gravitational interactions of the star and planets, the direct numerical orbit integrations presented below include one of the following effects: forced orbital migration, a change in m_1/m_2, or a change in $m_1 + m_2$. We change m_1/m_2 according to $d\ln(m_1/m_2)/dt = \text{constant}$ and keep $m_1 + m_2$ constant for the calculations with a change in m_1/m_2, and vice versa for the calculations with a change in $m_1 + m_2$. For the calculations with forced orbital migration (and constant masses), we force the outer planet to migrate inward with a migration rate of the form $\dot{a}_2/a_2 \propto P_2^{-1}$. The migration rate in equation (4) is of this form if α and H/a are independent of a. This form of the migration rate also has the convenient property that the evolution of systems with different initial outer semimajor axis $a_{2,0}$ but the same initial a_1/a_2 is independent of $a_{2,0}$ if we express the semimajor axes in units of $a_{2,0}$ and time in units of the initial outer orbital period $P_{2,0}$. Except for the migration calculations discussed in the last paragraph of § 3.2, there is no eccentricity damping.

The direct numerical orbit integrations were performed using modified versions of the symplectic integrator SyMBA (Duncan et al. 1998). SyMBA is based on a variant of the Wisdom & Holman (1991) method and employs a multiple–time step technique to handle close encounters. The latter feature is essential for the integrations that involve intersecting orbits and/or become unstable. Lee & Peale (2002) have described in detail how SyMBA can be modified to include forced migration and eccentricity damping. If there is no eccentricity damping, a single step of the modified algorithm starts with changing a_2 according to the forced migration term for half a time step, then evolving the system for a full time step using the original SyMBA algorithm, and then changing a_2 according to the forced migration term for another half–time step. For the calculations with a change in m_1/m_2 or

$m_1 + m_2$, we modify SyMBA to include the change in m_1/m_2 or $m_1 + m_2$ in the same manner as the forced migration term.

Unlike the calculations in Lee & Peale (2002), which used astrocentric orbital elements, ours have input and output in Jacobi orbital elements, and we apply the forced migration term to the Jacobi a_2 in the differential migration calculations. Lee & Peale (2003b) have shown that Jacobi elements should be used in the analysis of hierarchical planetary systems where a_1/a_2 is small and that the use of astrocentric elements can introduce significant high-frequency variations in orbital elements that should be nearly constant on orbital timescales. We have found through experiments that Jacobi elements are useful even for 2:1–resonant systems with $a_1/a_2 \approx 2^{-2/3}$. In their differential migration calculations for the GJ 876 system with $(m_1 + m_2)/m_0 = 0.0095$, Lee & Peale (2002) did not see the libration of θ_2 about 180°, which is expected for small eccentricities. However, when we repeated the calculations in Jacobi coordinates, we were able to see the libration of θ_2 about 180° at small eccentricities with the reduced fluctuations in the orbital elements (see also § 3.2 below).

3. RESONANCE CONFIGURATIONS FROM DIFFERENTIAL MIGRATION OF PLANETS WITH CONSTANT MASSES

3.1. *Results for* $(m_1 + m_2)/m_0 = 10^{-3}$ *and* $\dot{a}_2/a_2 = -10^{-6}/P_2$

We begin with a series of differential migration calculations, with m_1/m_2 ranging from 0.1 to 10. The total planetary mass $(m_1 + m_2)/m_0 = 10^{-3}$. The planets are initially on circular orbits, with the ratio of the semimajor axes $a_1/a_2 = 1/2$ (far from the 2:1 mean-motion commensurability), and the outer planet is forced to migrate inward at the rate $\dot{a}_2/a_2 = -10^{-6}/P_2$. The small total planetary mass [compared to $(m_1 + m_2)/m_0 \approx 10^{-2}$ of the GJ 876 system] and slow migration rate (compared to eq. [4] with the nominal parameter values) are chosen to reduce the libration amplitudes. The slow migration rate is also chosen to reduce the offsets in the centers of libration of the resonance variables due to the forced migration. The effects of a migration rate similar to that in equation (4) and a larger total planetary mass are discussed in § 3.2.

Figure 1 shows the evolution of the semimajor axes a_j, eccentricities e_j, and resonance variables θ_1 and θ_2 for the calculation with $m_1/m_2 = 0.3$ (which is close to $m_1/m_2 = 0.32$ of the GJ 876 system). As the outer planet migrates inward, the 2:1 mean-motion commensurability is encountered, and the system is first captured into the 2:1 resonance configuration with θ_1 librating about 0° and θ_2 about 180° (as in the Io-Europa pair). Continued migration forces e_1 to larger values and e_2 from increasing to decreasing until $e_2 \approx 0$ when $e_1 \approx 0.1$ (see Fig. 5*b* for a better view of this behavior). Then the system passes smoothly over to the configuration with both θ_1 and θ_2 librating about 0° (as in the GJ 876 system), and both e_1 and e_2 increase smoothly. The system remains stable for e_1 up to 0.8, when the calculation was terminated, although it may become unstable at larger e_1. In Figure 2*a*, we show the antisymmetric resonance configuration with $\theta_1 \approx 0°$ and $\theta_2 \approx 180°$. The eccentricities of the ellipses representing the orbits are exaggerated so that the positions of the periapses (marked by the dashes) are more visible. The planets (represented by the small dots) are shown at conjunction. The periapses are nearly antialigned, and conjunctions occur when the inner planet is near periapse and the outer planet is near apoapse. In Figure 2*b*, we show the symmetric resonance configuration with $\theta_1 \approx \theta_2 \approx 0°$. The eccentricities are for the configuration near $t/P_{2,0} = 6 \times 10^5$ in Figure 1. The periapses are nearly aligned, and conjunctions occur when both planets are near periapse. The evolution shown in Figure 1 is characteristic for $m_1/m_2 \lesssim 0.95$.

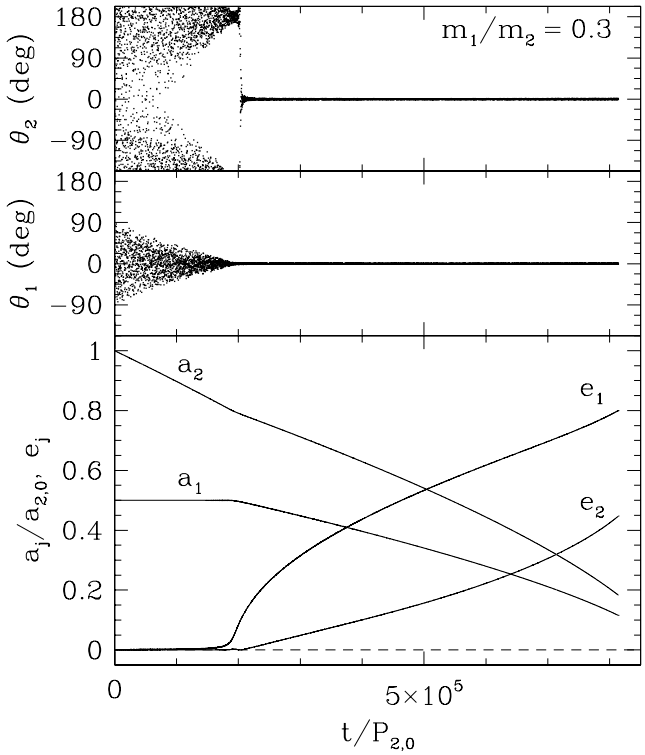

FIG. 1.—Evolution of the semimajor axes a_1 and a_2, eccentricities e_1 and e_2, and 2:1 mean-motion resonance variables $\theta_1 = \lambda_1 - 2\lambda_2 + \varpi_1$ and $\theta_2 = \lambda_1 - 2\lambda_2 + \varpi_2$, for a differential migration calculation with $m_1/m_2 = 0.3$ and $(m_1 + m_2)/m_0 = 10^{-3}$. The outer planet is forced to migrate inward with $\dot{a}_2/a_2 = -10^{-6}/P_2$. The semimajor axes and time are in units of the initial orbital semimajor axis, $a_{2,0}$, and period, $P_{2,0}$ of the outer planet, respectively. The sequence of resonance configurations after resonance capture is $(\theta_1, \theta_2) \approx (0°, 180°) \rightarrow (0°, 0°)$.

Figure 3 shows the evolution for the calculation with $m_1/m_2 = 1.5$. The capture into the $\theta_1 \approx 0°$ and $\theta_2 \approx 180°$ configuration and the passage to the $\theta_1 \approx \theta_2 \approx 0°$ configuration are as for $m_1/m_2 = 0.3$ in Figure 1. However, when the increasing e_1 reaches ≈0.17, the libration centers depart by tens of degrees from 0°, leading to stable libration of the θ_j far from either 0° or 180°. Asymmetric librations persist for $0.17 \lesssim e_1 \lesssim 0.44$, while e_2 changes from increasing to decreasing with increasing e_1. The system returns to the configuration with both θ_1 and θ_2 librating about 0° and both e_1 and e_2 increasing smoothly for sufficiently large e_1 ($\gtrsim$0.44). In Figure 2*c*, we show the asymmetric resonance configuration near $t/P_{2,0} = 4 \times 10^5$ in Figure 3. The angle between the lines of apsides is slightly more than 90°, and conjunctions occur when neither planet is near periapse or apoapse. It should be noted that conjunction means equal *true* longitudes of the planets, which is not the same as equal mean longitudes when θ_1 and θ_2 are not 0° or 180°. The evolution shown in Figure 3 is characteristic for $0.95 \lesssim m_1/m_2 \lesssim 2.55$, with the minimum (maximum) e_1 for asymmetric librations smaller (larger) for larger m_1/m_2 (see also Fig. 5*a*).

There appears to be a narrow range in m_1/m_2 ($2.55 \lesssim m_1/m_2 \lesssim 2.75$) for which the system changes from $\theta_1 \approx 0°$

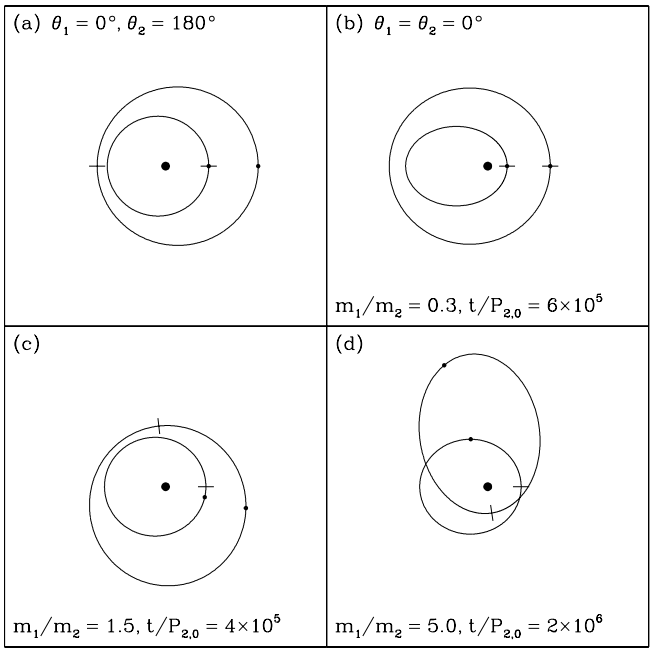

FIG. 2.—Examples of 2:1 resonance configurations that can be reached by differential migration of planets with constant masses and initially nearly circular orbits. The dashes on the ellipses representing the orbits mark the positions of the periapses, and the planets, represented by the small dots, are shown at conjunction. (*a*) Antisymmetric configuration with $\theta_1 \approx 0°$ and $\theta_2 \approx 180°$ at small eccentricities. The eccentricities of the orbits are exaggerated so that the positions of the periapses are more visible. (*b*) Symmetric configuration with $\theta_1 \approx \theta_2 \approx 0°$ near $t/P_{2,0} = 6 \times 10^5$ in Fig. 1. (*c*) Asymmetric configuration near $t/P_{2,0} = 4 \times 10^5$ in Fig. 3. (*d*) Asymmetric configuration with intersecting orbits near $t/P_{2,0} = 2 \times 10^6$ in Fig. 4.

and $\theta_2 \approx 180°$ to asymmetric librations without passing through the $\theta_1 \approx \theta_2 \approx 0°$ configuration as e_1 increases, but the system does return to the $\theta_1 \approx \theta_2 \approx 0°$ configuration for sufficiently large e_1. Figure 4 shows the evolution for the calculation with $m_1/m_2 = 5$, which is characteristic for $m_1/m_2 \gtrsim 2.75$. The system changes from $\theta_1 \approx 0°$ and $\theta_2 \approx 180°$ to asymmetric librations and never reaches the $\theta_1 \approx \theta_2 \approx 0°$ configuration. In the asymmetric libration branch, e_2 increases monotonically with time but e_1 does not. The system eventually becomes unstable at $t/P_{2,0} = 2.06 \times 10^6$. The asymmetric libration configurations in Figure 4 with $e_2 \gtrsim 0.35$ have the additional property that the orbits intersect. An example—the configuration near $t/P_{2,0} = 2 \times 10^6$—is shown in Figure 2*d*.

It should be noted that the symmetries of the problem without forced migration mean that every stable 2:1 resonance configuration with centers of libration about θ_1 and θ_2 has a counterpart with $-\theta_1$ and $-\theta_2$. However, the forced migration causes small offsets in the libration centers, and there could be a preference for evolution into one of the asymmetric libration branches, depending on the migration rate and the libration amplitudes. As in the examples shown in Figures 3 and 4, all of our calculations that yielded asymmetric configurations have θ_1 becoming negative when θ_1 initially departs from 0°.

A convenient and informative way to summarize the results for different m_1/m_2 is to plot the trajectories in the e_1-e_2 plane (Beaugé et al. 2003; Ferraz-Mello et al. 2003). Figure 5 shows the trajectories for several values of m_1/m_2 between 0.1 and 10, with Figure 5*a* in linear scales and Figure 5*b* showing the small eccentricity region in logarithmic scales. The trajectories for $m_1/m_2 \lesssim 0.95$, $0.95 \lesssim m_1/m_2 \lesssim 2.55$, $2.55 \lesssim m_1/m_2 \lesssim 2.75$, and $m_1/m_2 \gtrsim 2.75$ [with the sequences of libration centers (θ_1, θ_2) summarized in Table 1] are clearly distinguished in the e_1-e_2 plane. The transition from $(\theta_1, \theta_2) \approx (0°, 180°)$ at small eccentricities to $(\theta_1, \theta_2) \approx (0°, 0°)$ for $m_1/m_2 \lesssim 2.55$ occurs when $e_1 \approx 0.1$ and $e_2 \approx 0$, and the transition to

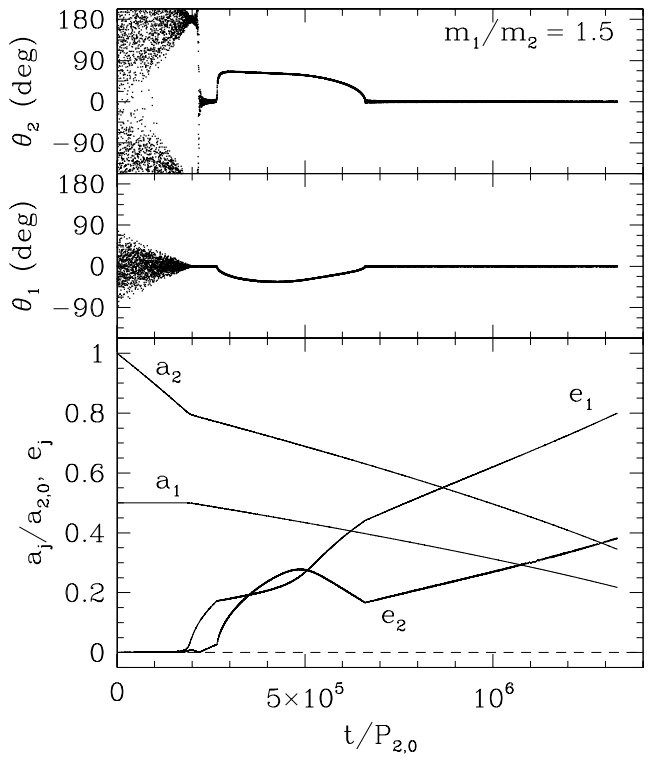

FIG. 3.—Same as Fig. 1, but for $m_1/m_2 = 1.5$. The sequence of resonance configurations after resonance capture is $(\theta_1, \theta_2) \approx (0°, 180°) \rightarrow (0°, 0°) \rightarrow$ asymmetric librations $\rightarrow (0°, 0°)$.

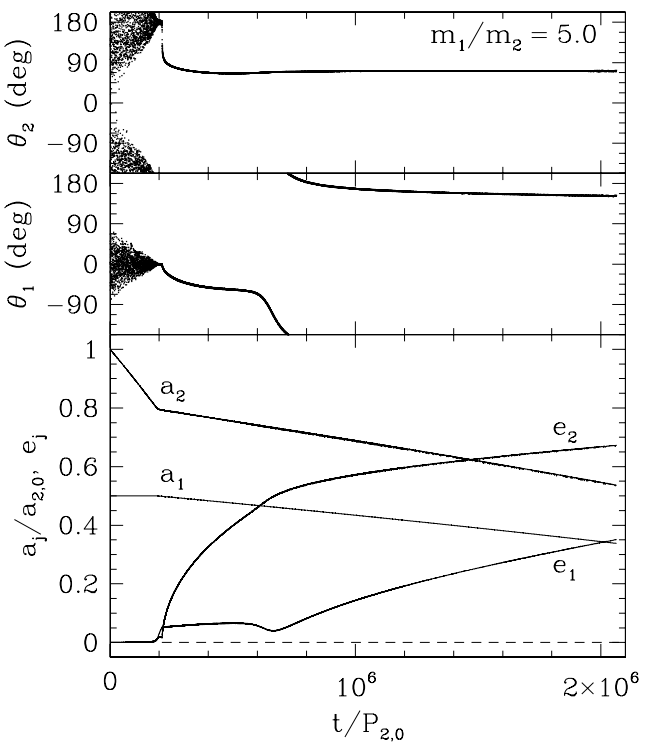

FIG. 4.—Same as Fig. 1, but for $m_1/m_2 = 5$. The sequence of resonance configurations after resonance capture is $(\theta_1, \theta_2) \approx (0°, 180°) \rightarrow$ asymmetric librations.

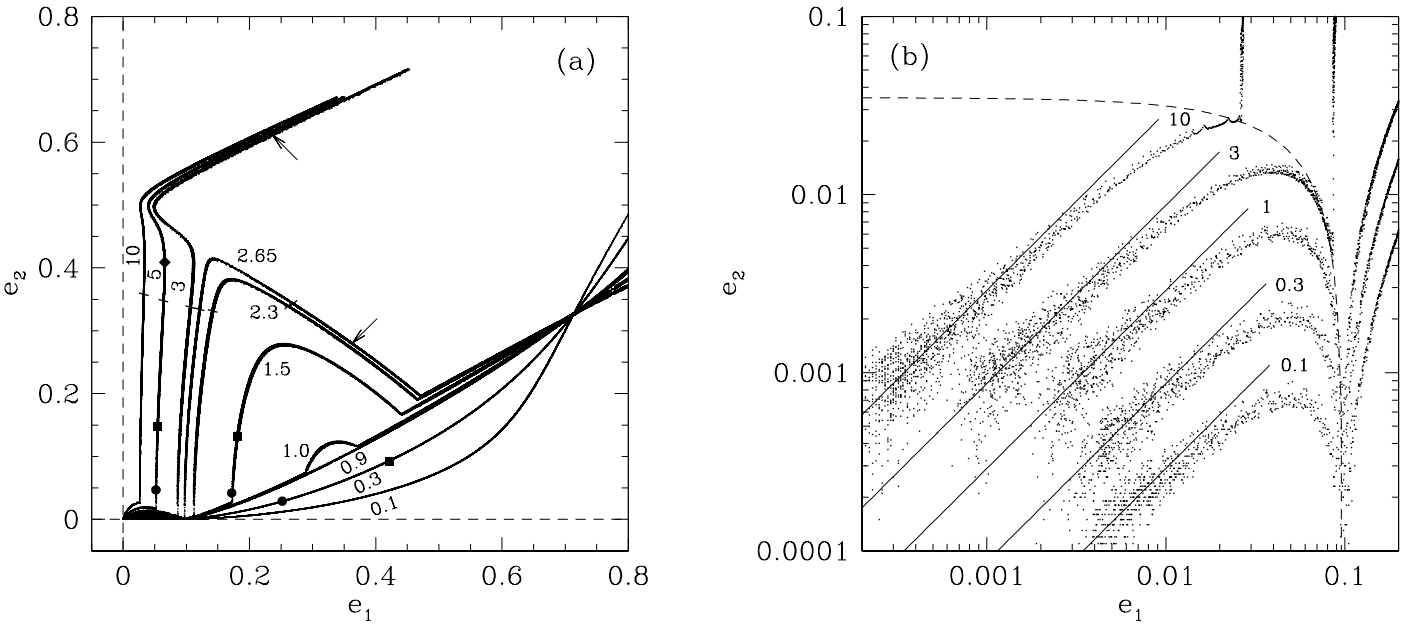

FIG. 5.—Trajectories of 2:1 resonance configurations from differential migration of planets with constant masses and initially nearly circular orbits. The trajectories are labeled by m_1/m_2. The total planetary mass $(m_1 + m_2)/m_0 = 10^{-3}$, and the outer planet is forced to migrate inward with $\dot{a}_2/a_2 = -10^{-6}/P_2$. (*a*) The e_1-e_2 plane in linear scales. The configurations above the dash for $m_1/m_2 = 3$, 5, and 10 and the configurations between the two dashes for $m_1/m_2 = 2.3$ and 2.65 have intersecting orbits. The diamond, squares, and circles on the curves with $m_1/m_2 = 0.3$, 1.5, and 5 indicate the equilibrium eccentricities for eccentricity damping of the outer planet with $K = |\dot{e}_2/e_2|/|\dot{a}_2/a_2| = 1$, 10, and 100, respectively. See text for $K = 1$ and $m_1/m_2 = 0.3$ and 1.5. The configurations indicated by the arrows on the curves with $m_1/m_2 = 2.65$ and 3 are used as initial conditions for calculations in § 3.2 and Figs. 7 and 8. (*b*) The small eccentricity region of the e_1-e_2 plane in logarithmic scales. The solid lines show the relationship in eq. (7) from the resonant perturbation theory to the lowest order in the eccentricities. The dashed line is for the boundary below which the $\theta_1 = 0^\circ$ and $\theta_2 = 180^\circ$ configuration exists, as determined by Beaugé et al. (2003).

asymmetric librations for $m_1/m_2 \gtrsim 2.55$ occurs before e_1 reaches 0.1, with the critical value of e_1 smaller for larger m_1/m_2 (see Fig. 5*b*). Beaugé et al. (2003) have determined the boundary in e_1-e_2 space below which the $\theta_1 = 0^\circ$ and $\theta_2 = 180^\circ$ configuration exists, using an analytic model for the resonant Hamiltonian (with an expansion in eccentricities). Their result is well approximated by the relationship $e_2 = -0.36e_1 + 0.035$, which is shown as the dashed line in Figure 5*b*. It is in good agreement with the boundary in our numerical results.

For coplanar orbits, the equation for the variation of the periapse longitude is

$$\frac{d\varpi_j}{dt} = -\frac{\sqrt{1 - e_j^2}}{m_j e_j \sqrt{G m_0 a_j}} \frac{\partial \Phi}{\partial e_j}, \tag{5}$$

where the disturbing potential

$$\Phi = -\frac{G m_1 m_2}{a_2} \varphi(\beta, e_1, e_2, \theta_1, \theta_2), \tag{6}$$

φ is a function of the indicated variables, and $\beta = a_1/a_2 \approx 2^{-2/3}$, if we consider only the resonant terms and neglect terms of order $[(m_1 + m_2)/m_0]^2$ and higher (see, e.g., Lee & Peale 2002; Beaugé & Michtchenko 2003). To the lowest order in the eccentricities, $d\varpi_1/dt = \beta n_1 (m_2/m_0) C_1/e_1$ and $d\varpi_2/dt = -n_2 (m_1/m_0) C_2/e_2$ for $\theta_1 = 0^\circ$ and $\theta_2 = 180^\circ$, where n_j are the mean motions and $C_1(\beta) = -1.19$ and $C_2(\beta) = +0.43$ are, respectively, the coefficients of the $e_1 \cos\theta_1$ and $e_2 \cos\theta_2$ terms of the disturbing potential (Lee & Peale 2002). Thus, for 2:1 resonance configurations with sufficiently small eccentricities, the precessions of the orbits are retrograde, and the requirement that the orbits on average precess at the same rate implies the following relationship between the forced eccentricities:

$$e_2/e_1 = -\beta^{1/2} (C_2/C_1)(m_1/m_2) = 0.29(m_1/m_2). \tag{7}$$

Our numerical results have finite widths in e_1 and e_2 as a result of finite libration amplitudes, but they are on average in good agreement with equation (7) (Fig. 5*b*, *solid lines*) for sufficiently small eccentricities. We terminate the solid lines in Figure 5*b* at $e_1 = 0.12/(m_1/m_2 + 3)$, which is an estimate of where significant deviation from equation (7) would occur,

TABLE 1

SEQUENCES OF 2:1 RESONANCE CONFIGURATIONS FROM DIFFERENTIAL MIGRATION OF PLANETS WITH CONSTANT MASSES

Planetary Mass Ratio	Libration Centers (θ_1, θ_2)
$m_1/m_2 \lesssim 0.95$	$(0^\circ, 180^\circ) \rightarrow (0^\circ, 0^\circ)$
$0.95 \lesssim m_1/m_2 \lesssim 2.55$	$(0^\circ, 180^\circ) \rightarrow (0^\circ, 0^\circ) \rightarrow$ asymmetric librations $\rightarrow (0^\circ, 0^\circ)$
$2.55 \lesssim m_1/m_2 \lesssim 2.75$	$(0^\circ, 180^\circ) \rightarrow$ asymmetric librations $\rightarrow (0^\circ, 0^\circ)$
$2.75 \lesssim m_1/m_2$	$(0^\circ, 180^\circ) \rightarrow$ asymmetric librations

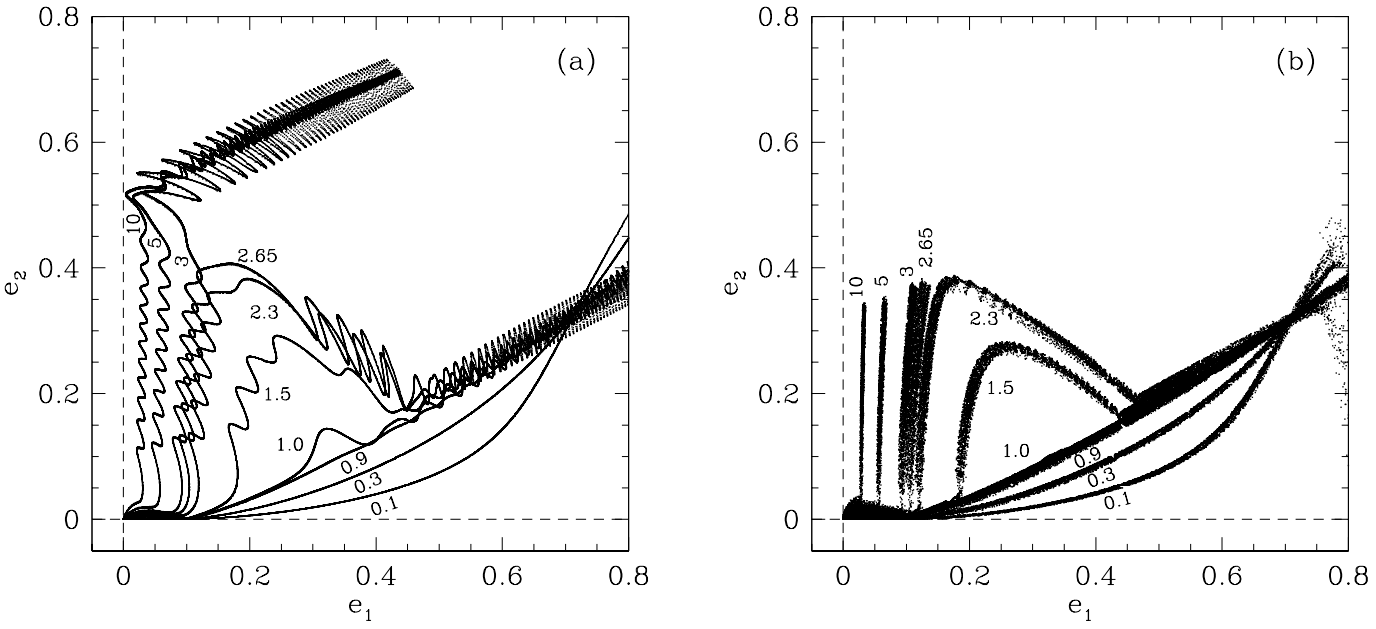

FIG. 6.—Same as Fig. 5*a*, but for $\dot{a}_2/a_2 = -10^{-4}/P_2$ and (*a*) $(m_1 + m_2)/m_0 = 10^{-3}$ and (*b*) $(m_1 + m_2)/m_0 = 10^{-2}$. The basic trajectories depend only on m_1/m_2, but the libration amplitudes and the point at which a sequence becomes unstable can be sensitive to the migration rate and the total planetary mass.

based on the position of the local maximum of e_2 for $m_1/m_2 \ll 1$ and the boundary in e_1-e_2 space for the $\theta_1 = 0^\circ$ and $\theta_2 = 180^\circ$ configuration.

As we just mentioned, the orbital precessions are retrograde for the resonance configurations with small eccentricities. The precessions remain retrograde throughout the trajectories shown in Figure 5*a* for $m_1/m_2 \gtrsim 2.75$. On the other hand, all of the trajectories for $m_1/m_2 \lesssim 2.75$ pass through a point with $e_1 = 0.714$ and $e_2 = 0.326$, where $d\varpi_1/dt = d\varpi_2/dt = 0$ and the precessions of the orbits change from retrograde to prograde. (Lee & Peale 2002 have already noted the change from retrograde to prograde precessions for systems with masses like those in GJ 876.) According to equations (5) and (6), the masses only appear as overall factors in $d\varpi_j/dt$, with $d\varpi_1/dt \propto m_2/(m_0)^{1/2}$ and $d\varpi_2/dt \propto m_1/(m_0)^{1/2}$. Thus, for small-amplitude librations and nearly constant e_j and θ_j, the combinations of e_j and θ_j for which $d\varpi_1/dt = d\varpi_2/dt$ is nonzero depend only on m_1/m_2, and the combinations for which $d\varpi_1/dt = d\varpi_2/dt = 0$ are independent of the planetary and stellar masses. Since all of the cases in Figure 5*a* with $m_1/m_2 \lesssim 2.75$ have θ_1 and θ_2 librating about 0° at large e_1, the only point on the e_1-e_2 plane where the trajectories can intersect is a combination of e_1 and e_2 for which $d\varpi_1/dt = d\varpi_2/dt = 0$.

In our discussion above of the case with $m_1/m_2 = 5$, we pointed out that the asymmetric libration configurations with $e_2 \gtrsim 0.35$ have intersecting orbits (see, e.g., Fig. 2*d*). Ferraz-Mello et al. (2003) have stated that configurations with the apocentric distance of the inner planet greater than the pericentric distance of the outer planet [i.e., $a_1(1 + e_1) > a_2(1 - e_2)$ for $m_1, m_2 \ll m_0$] may have intersecting orbits, but this condition is necessary but not sufficient (it is both necessary and sufficient only for antialigned configurations, such as those discussed in § 4.2). We have determined which of the configurations shown in Figure 5*a* actually have intersecting orbits. For $m_1/m_2 = 3$, 5, and 10, the configurations above the dash on each trajectory have intersecting orbits. However, configurations with intersecting orbits are not limited to $m_1/m_2 \gtrsim 2.75$. For $m_1/m_2 = 2.3$ and 2.65, the configurations between the two dashes on each trajectory also have intersecting orbits.

3.2. *Effects of Migration Rate, Total Planetary Mass, and Eccentricity Damping*

We consider next the effects of a migration rate on the disk viscous timescale similar to that in equation (4) and a larger total planetary mass. We have performed differential migration calculations similar to those in § 3.1, but with $\dot{a}_2/a_2 = -10^{-4}/P_2$ and $(m_1 + m_2)/m_0 = 10^{-3}$ and 10^{-2}, and the trajectories of stable resonance configurations in the e_1-e_2 plane are shown in Figures 6*a* and 6*b*, respectively. Figures 5*a* and 6 show that the basic trajectories depend only on m_1/m_2 and not on the total planetary mass, in agreement with the analysis in § 3.1 based on the requirement of equal precession rates. However, the libration amplitudes and the point at which a sequence becomes unstable can be sensitive to the migration rate and the total planetary mass.

For $(m_1 + m_2)/m_0 = 10^{-3}$, the faster migration rate (Fig. 6*a*) leads to larger libration amplitudes when a system with $m_1/m_2 \gtrsim 0.95$ enters asymmetric libration, and the point at which a system with $m_1/m_2 \gtrsim 2.75$ becomes unstable is slightly different from that shown in Figure 5*a*. All of the trajectories in Figure 6*b* for $(m_1 + m_2)/m_0 = 10^{-2}$ are wider than those in Figure 5*a*, because the larger eccentricity variations generated by the larger total planetary mass before resonance capture lead to resonance configurations with larger libration amplitudes. On the other hand, although the trajectories in Figures 6*a* and 6*b* are for the same migration rate, those in Figure 6*b* with $m_1/m_2 \gtrsim 0.95$ do not show any significant increase in the libration amplitudes when a system enters asymmetric libration, because the larger total planetary mass means that the resonant interaction between the planets is stronger relative to the forced migration. It is not clear in Figure 6*b*, but with the use of Jacobi coordinates (see § 2), we are able to see the capture into the $\theta_1 \approx 0^\circ$ and $\theta_2 \approx 180^\circ$ configuration at small eccentricities when we examine time evolution plots (like those in Figs. 1, 3, and 4) for these calculations with $(m_1 + m_2)/m_0 = 10^{-2}$.

In Figure 6*b*, many of the trajectories for $m_1/m_2 \leq 2.3$ show deviations from the trajectories in Figure 5*a* at $e_1 \gtrsim 0.75$ due to rapid increase in the libration amplitudes before the system becomes unstable (see § 4.1 for a more detailed discussion of a similar case). The cases with $m_1/m_2 \geq 2.65$ become unstable near the points where the orbits become intersecting (dashes on the trajectories in Fig. 5*a*). Note, however, that the case with $m_1/m_2 = 2.3$ passes through the configurations with intersecting orbits without becoming unstable. The fact that a sequence becomes unstable at a certain point does not mean that all configurations beyond that point are necessarily unstable, especially for smaller libration amplitudes. We have used the asymmetric configuration with nonintersecting orbits, indicated by the arrow on the curve with $m_1/m_2 = 2.65$ in Figure 5*a*, as the starting point for a calculation in which $m_1 + m_2$ is increased from $10^{-3}m_0$ at a rate of $d\ln(m_1 + m_2)/dt = 10^{-6}/P_{2,0}$ while m_1/m_2 is kept constant. It remains stable to the end of the calculation when $(m_1 + m_2)/m_0 = 10^{-2}$. When we use instead the asymmetric configuration with intersecting orbits, indicated by the arrow on the curve with $m_1/m_2 = 3$ in Figure 5*a*, as the starting point, the configuration becomes unstable when $(m_1 + m_2)/m_0$ exceeds 0.0033.

As we mentioned in § 1, either eccentricity damping or the termination of migration due to nebula dispersal would lead to a system's being left somewhere along a sequence in Figures 5 and 6. There is significant uncertainty in both the sign and the magnitude of the net effect of planet-disk interaction on the orbital eccentricity of the planet because of sensitivity to the distribution of disk material near the locations of the Lindblad and corotation resonances (e.g., Goldreich & Sari 2003). Nevertheless, hydrodynamic simulations of two planets orbiting inside an outer disk have shown eccentricity damping of the outer planet, with $K = |\dot{e}_2/e_2|/|\dot{a}_2/a_2| \sim 1$ (Kley et al. 2004), while an explanation of the observed eccentricities of the GJ 876 system as equilibrium eccentricities requires $K \sim 100$ (Lee & Peale 2002). To study the effects of eccentricity damping, we have repeated the $m_1/m_2 = 0.3$, 1.5, and 5 calculations shown in Figures 1, 3, and 4 with $K = 1$, 10, and 100. For $K = 10$ and 100, the eccentricities reach equilibrium values in all cases, and they are indicated by the squares and circles in Figure 5*a*. For $K = 1$, while the eccentricities in the $m_1/m_2 = 5$ calculation reach equilibrium values indicated by the diamond in Figure 5*a*, those in the $m_1/m_2 = 0.3$ and 1.5 calculations are still increasing at the end of the calculations when $e_1 \approx 0.68$ and 0.70, respectively.

4. OTHER RESONANCE CONFIGURATIONS

4.1. *Symmetric and Asymmetric Configurations*

The bifurcation of the trajectories in Figure 5*a* at $m_1/m_2 \approx 2.75$ leaves an empty region in the e_1-e_2 plane. In this subsection, we show that there are stable 2:1 resonance configurations in the empty region of Figure 5*a* that cannot be reached by the scenario considered in § 3 (i.e., differential migration of planets with constant masses and initially nearly circular orbits).

In Figure 7, we show the results of a calculation in which the asymmetric configuration indicated by the arrow on the curve with $m_1/m_2 = 3$ in Figure 5*a* is used as the starting point and m_1/m_2 is decreased from 3 to 0.1 at a rate of $d\ln(m_1/m_2)/dt = -10^{-6}/P_{2,0}$ while $(m_1 + m_2)/m_0 = 10^{-3}$ is kept constant. As m_1/m_2 decreases, θ_1 and θ_2 remain near the initial values, e_2 changes little, and e_1 increases (i.e., the sequence extends to the right in the e_1-e_2 plane). Similarly, we

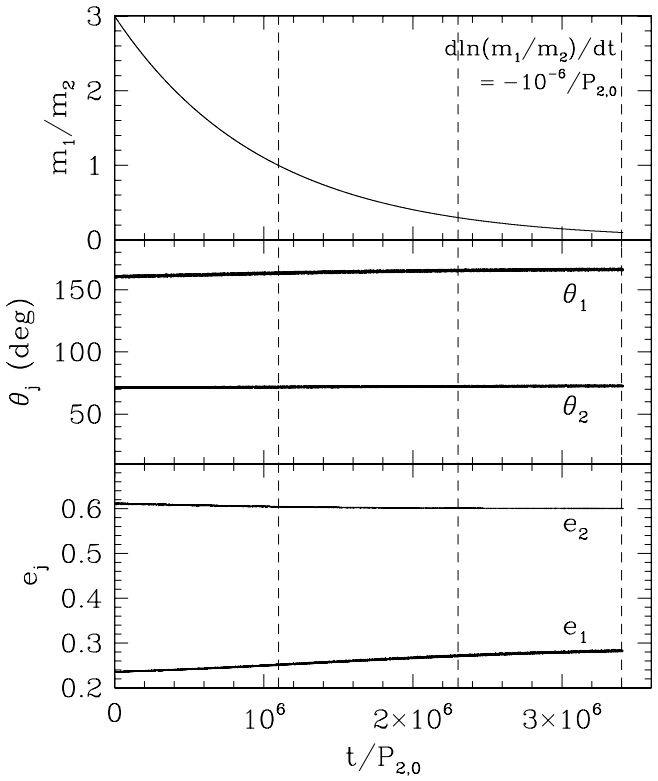

FIG. 7.—Evolution of the eccentricities e_1 and e_2, mean-motion resonance variables θ_1 and θ_2, and mass ratio m_1/m_2 for a calculation in which the configuration indicated by the arrow on the curve with $m_1/m_2 = 3$ in Fig. 5*a* is used as the starting point and m_1/m_2 is decreased at a rate of $d\ln(m_1/m_2)/dt = -10^{-6}/P_{2,0}$. The configurations with $m_1/m_2 = 1$, 0.3, and 0.1, indicated by the dashed lines, are used as initial conditions for calculations in Figs. 9 and 11 and § 4.3.

have used the asymmetric configuration indicated by the arrow on the curve with $m_1/m_2 = 2.65$ in Figure 5*a* as the starting point for a calculation in which m_1/m_2 is increased from 2.65 to 10 at a rate of $d\ln(m_1/m_2)/dt = 10^{-6}/P_{2,0}$. The results are shown in Figure 8. As m_1/m_2 increases, θ_1 and θ_2 remain near the initial values, e_1 changes little, and e_2 increases (i.e., the sequence extends upward in the e_1-e_2 plane). Thus, we have found for each m_1/m_2 between 0.1 and 10 a resonance configuration distinct from those shown in Figure 5*a*.

For a given m_1/m_2, we can then use the resonance configuration from either Figure 7 (if $m_1/m_2 \lesssim 2.75$) or Figure 8 (if $m_1/m_2 \gtrsim 2.75$) as the starting point for "forward" ($\dot{a}_2/a_2 < 0$) and "backward" ($\dot{a}_2/a_2 > 0$) migration calculations to search for other resonance configurations. Figure 9 shows the results from the $m_1/m_2 = 0.3$ calculations with $\dot{a}_2/a_2 = -10^{-6}/P_2$ and $10^{-6}/P_2$ along the positive and negative time axes, respectively. In both calculations we have integrated the system until it becomes unstable. The asymmetric resonance configurations in Figure 9 are clearly different from the symmetric and antisymmetric configurations in Figure 1. Figure 10 shows the results from the $m_1/m_2 = 5$ calculations. The calculation with $\dot{a}_2/a_2 = -10^{-6}/P_2$ was terminated when e_1 reached 0.8, while the calculation with $\dot{a}_2/a_2 = 10^{-6}/P_2$ was terminated when both θ_1 and θ_2 circulated. We do not consider further configurations with only θ_2 librating, but it is interesting that those in Figure 10 at $-8.5 \times 10^5 \lesssim t/P_{2,0} \lesssim -4.6 \times 10^5$ are similar to those in Figure 4 at $t/P_{2,0} \lesssim 6 \times 10^5$ with both θ_1 and θ_2 librating. The configurations in Figure 10

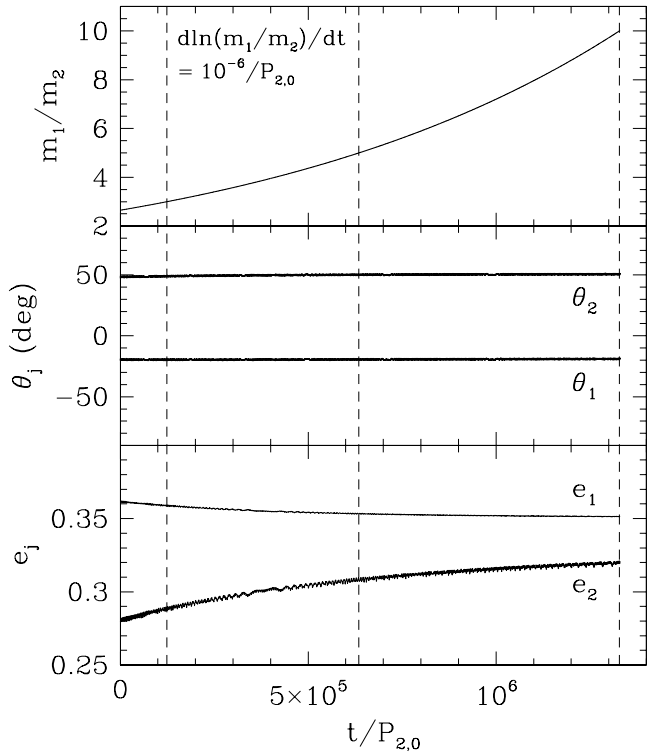

FIG. 8.—Same as Fig. 7, but for a calculation in which the configuration indicated by the arrow on the curve with $m_1/m_2 = 2.65$ in Fig. 5*a* is used as the starting point and m_1/m_2 is increased at a rate of $d\ln(m_1/m_2)/dt = 10^{-6}/P_{2,0}$. The configurations with $m_1/m_2 = 3$, 5, and 10, indicated by the dashed lines, are used as initial conditions for calculations in Figs. 10 and 11 and § 4.3.

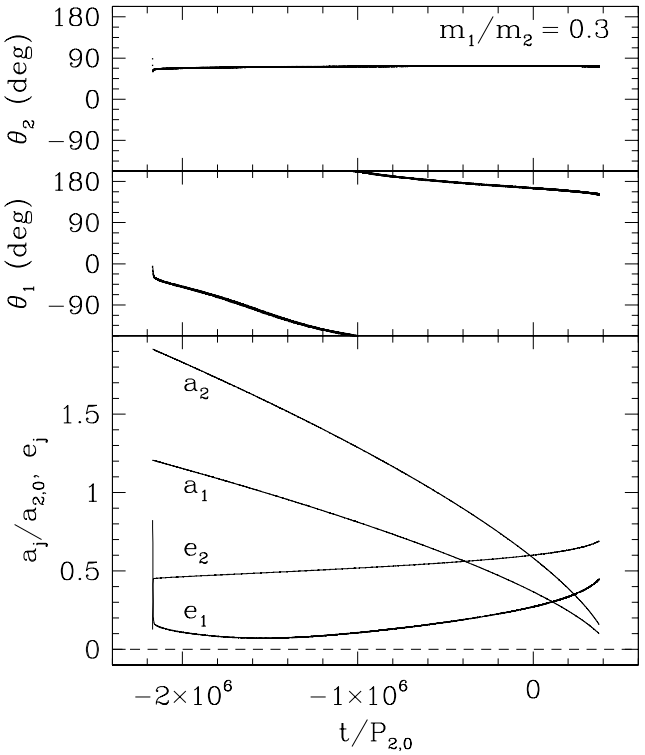

FIG. 9.—Resonance configurations from forward and backward migration calculations using the $m_1/m_2 = 0.3$ configuration from Fig. 7 as initial conditions. The results from the calculations with $\dot{a}_2/a_2 = -10^{-6}/P_2$ and $10^{-6}/P_2$ are plotted along the positive and negative time axes, respectively. These resonance configurations are different from those in Fig. 1 from differential migration of planets with constant masses and initially nearly circular orbits.

with both θ_1 and θ_2 librating (at $t/P_{2,0} \gtrsim -4.6 \times 10^5$) are either symmetric or asymmetric, and they are clearly different from those in Figure 4.

In Figure 11, we show the trajectories in the e_1-e_2 plane of stable resonance configurations (with both θ_1 and θ_2 librating) from the forward and backward differential migration calculations with initial conditions (Fig. 11, *triangles*) from Figures 7 and 8 for $m_1/m_2 = 0.1$, 1, 3, and 10. The trajectories for $m_1/m_2 = 0.3$ and 5, whose time evolutions are shown in Figures 9 and 10, respectively, are simply between the appropriate pairs in Figure 11 and are not shown to avoid crowding. Unlike the cases with $m_1/m_2 = 3$ and 5 (see Fig. 10 for the latter), where e_2 increases monotonically with increasing e_1 for the $\theta_1 \approx \theta_2 \approx 0^\circ$ configurations at large e_1, the trajectory for $m_1/m_2 = 10$ shows a maximum in e_2 at $e_1 \approx 0.72$. This turns out to be due to the libration amplitudes of θ_1 and θ_2 becoming too large. As the example in Figure 10 shows, the libration amplitudes of θ_1 and θ_2 increase as the system is driven deeper into resonance. The semiamplitudes do not exceed 10° in the cases with $m_1/m_2 = 3$ and 5, but for $m_1/m_2 = 10$, the configurations with $e_1 \gtrsim 0.68$ have semiamplitudes of θ_1 and $\theta_2 > 10^\circ$ (although θ_1 and θ_2 are nearly in phase, so that the libration amplitude of $\theta_3 = \theta_1 - \theta_2$ remains small and the trajectory in the e_1-e_2 plane remains narrow). We have repeated the $m_1/m_2 = 10$ calculation by starting at $e_1 = 0.61$ with initial conditions that correspond to smaller libration amplitudes. The resulting trajectory is shown as the gray curve in Figure 11, and it does not show the decrease in e_2 at large e_1.

Like the trajectories in Figure 5*a* for $m_1/m_2 \lesssim 2.75$, the trajectories in Figure 11 for $m_1/m_2 = 3$ and 10 (the gray curve for the latter) also pass through the point with $e_1 = 0.714$ and

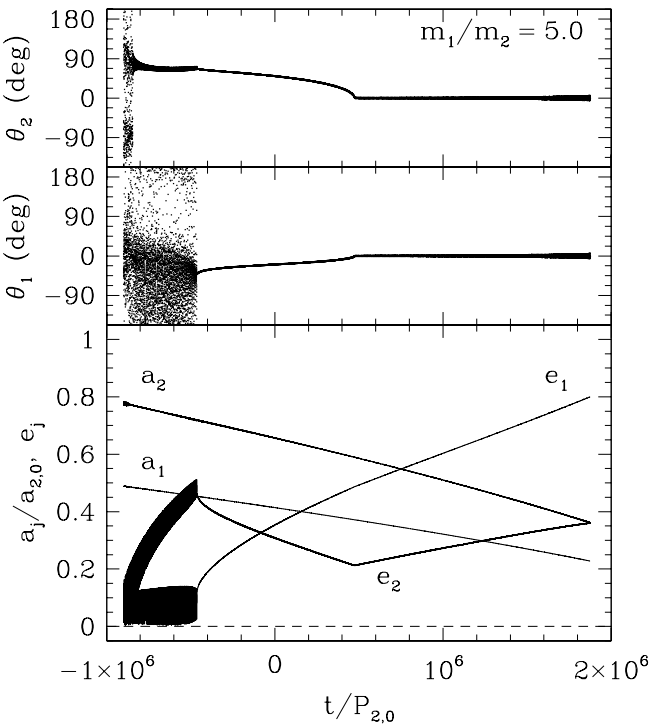

FIG. 10.—Same as Fig. 9, but for calculations using the $m_1/m_2 = 5$ configuration from Fig. 8 as initial conditions. The configurations at $t/P_{2,0} \gtrsim -4.6 \times 10^5$ with both θ_1 and θ_2 librating are different from those in Fig. 4.

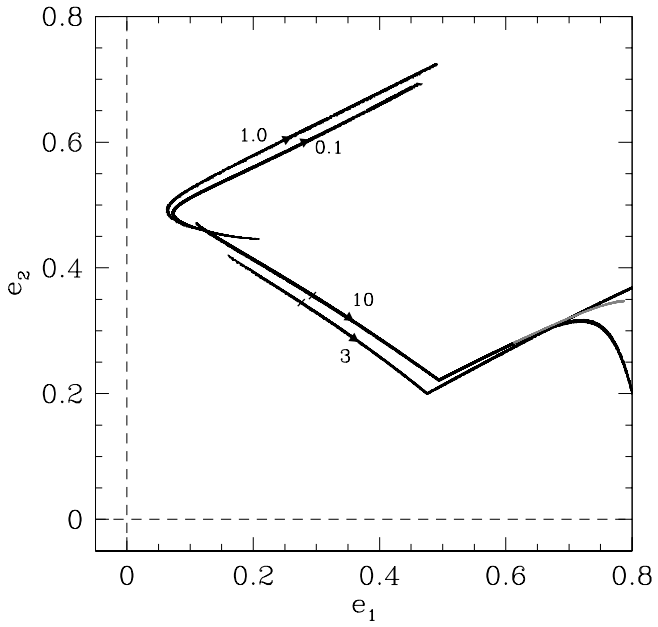

FIG. 11.—Trajectories in the e_1-e_2 plane of 2:1 resonance configurations from forward and backward migration calculations with initial conditions (*triangles*, *oriented to indicate the direction for forward migration*) from Figs. 7 and 8 for $m_1/m_2 = 0.1$, 1, 3, and 10. See text for the calculation that produces the gray curve for $m_1/m_2 = 10$. The resonance configurations are distinct from those in Fig. 5*a*. All of the configurations for $m_1/m_2 = 0.1$ and 1 and the configurations to the left of the dashes on the trajectories for $m_1/m_2 = 3$ and 10 have intersecting orbits.

$e_2 = 0.326$, where $d\varpi_1/dt = d\varpi_2/dt = 0$ and the precessions of the orbits change from retrograde at smaller e_1 to prograde at larger e_1. In Figure 11, all of the configurations for $m_1/m_2 = 0.1$ and 1 and the configurations to the left of the dashes on the trajectories for $m_1/m_2 = 3$ and 10 have intersecting orbits.

The configurations shown in Figure 11 clearly occupy a different part of the e_1-e_2 plane, compared to those in Figure 5*a*. They are found by a combination of calculations in which m_1/m_2 is changed slowly and differential migration calculations, and they cannot be reached by differential migration of planets with constant masses and initially nearly circular orbits.

4.2. *Antisymmetric Configurations with* $\theta_1 \approx 180^\circ$ *and* $\theta_2 \approx 0^\circ$

As we mentioned in § 1, Ji et al. (2003) and Hadjidemetriou & Psychoyos (2003) have discovered stable 2:1 resonance configurations with $\theta_1 \approx 180^\circ$ and $\theta_2 \approx 0^\circ$ for systems with masses similar to those announced initially by the Geneva group for the HD 82943 system [$m_1/m_2 = 0.54$, $(m_1 + m_2)/m_0 = 2.3 \times 10^{-3}$]. We have derived from the results of Ji et al. (2003) a $\theta_1 \approx 180^\circ$ and $\theta_2 \approx 0^\circ$ configuration with $m_1/m_2 = 0.54$, $(m_1 + m_2)/m_0 = 10^{-3}$, and small libration amplitudes, and it is shown in Figure 12. The $\theta_1 \approx 180^\circ$ and $\theta_2 \approx 0^\circ$ configuration has intersecting orbits, with the periapses nearly antialigned and conjunctions occurring when the inner planet is near apoapse and the outer planet is near periapse (and closer to the star than the inner planet).

We have used the configuration in Figure 12 as the starting point for calculations in which m_1/m_2 is increased to 10 and decreased to 0.1. The results are shown in Figure 13, with the calculations with $d\ln(m_1/m_2)/dt = 10^{-6}/P_{2,0}$ and $-10^{-6}/P_{2,0}$ along the positive and negative time axes, respectively. The libration centers remain at $\theta_1 = 180^\circ$ and $\theta_2 = 0^\circ$, and e_1 decreases (e_2 increases) with increasing m_1/m_2. We have thus

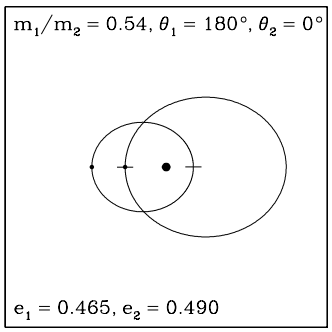

FIG. 12.—Antisymmetric resonance configuration with $\theta_1 \approx 180^\circ$, $\theta_2 \approx 0^\circ$, and intersecting orbits, used as the starting point for calculations in Fig. 13.

found for each m_1/m_2 in the range $0.1 \leq m_1/m_2 \leq 10$ a resonance configuration with $\theta_1 \approx 180^\circ$ and $\theta_2 \approx 0^\circ$. As in § 4.1, we can then use the resonance configuration for a given m_1/m_2 from Figure 13 as the starting point for forward and backward migration calculations to search for other resonance configurations with the same m_1/m_2. Figure 14 shows the trajectories in the e_1-e_2 plane of stable resonance configurations from the migration calculations with $m_1/m_2 = 0.1$, 1, and 10. The initial conditions (Fig. 14, *triangles*) are indicated by the dashed lines in Figure 13. The calculations with $\dot{a}_2/a_2 = -10^{-6}/P_2$ were terminated when e_2 reached 0.7, while the calculations with $\dot{a}_2/a_2 = 10^{-6}/P_2$ were terminated when the system became unstable. All of the configurations shown in Figure 14 have

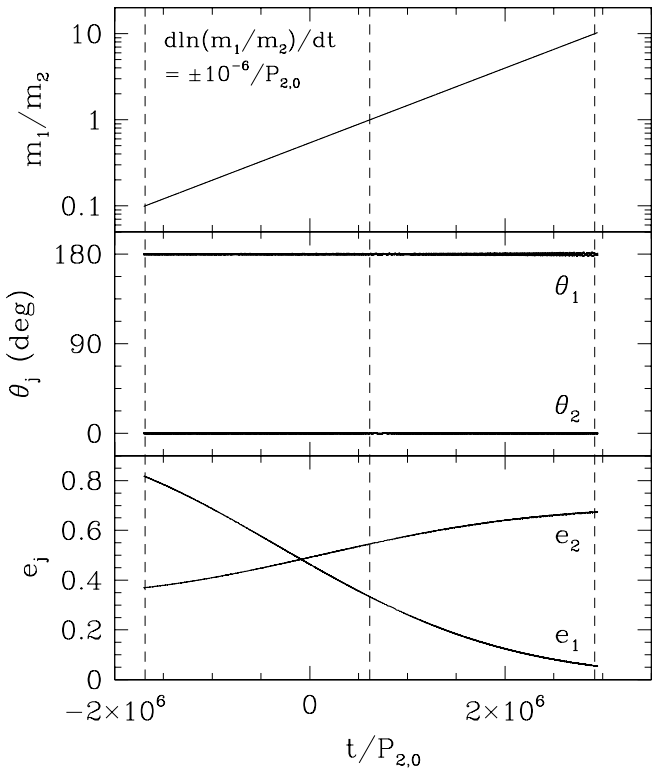

FIG. 13.—Evolution of the eccentricities e_1 and e_2, mean-motion resonance variables θ_1 and θ_2, and mass ratio m_1/m_2 for calculations in which the configuration shown in Fig. 12 is used as the starting point and m_1/m_2 is increased to 10 and decreased to 0.1. The results from the calculations with $d\ln(m_1/m_2)/dt = 10^{-6}/P_{2,0}$ and $-10^{-6}/P_{2,0}$ are plotted along the positive and negative time axes, respectively. The configurations with $m_1/m_2 = 0.1$, 1, and 10, indicated by the dashed lines, are used as initial conditions for calculations in Fig. 14.

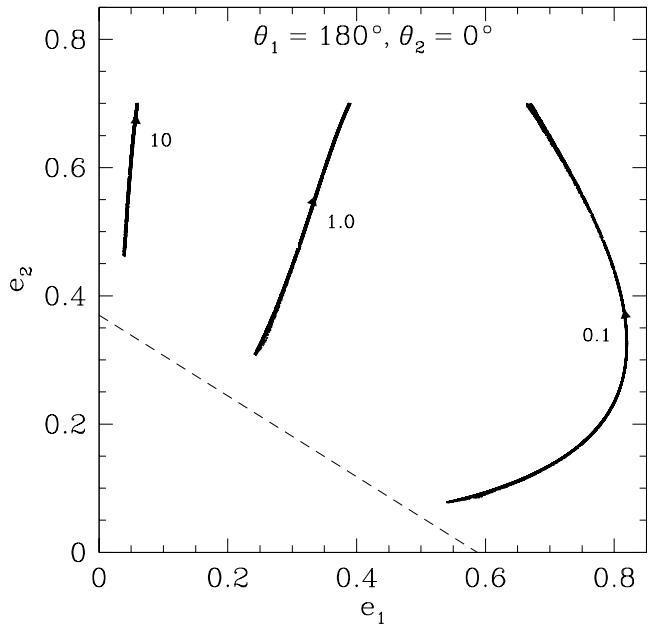

FIG. 14.—Trajectories in the e_1-e_2 plane of 2:1 resonance configurations with $\theta_1 \approx 180°$ and $\theta_2 \approx 0°$ from forward and backward migration calculations with initial conditions (*triangles*, *oriented to indicate the direction for forward migration*) from Fig. 13 for $m_1/m_2 = 0.1$, 1, and 10. These resonance configurations are distinct from those in Figs. 5*a* and 11. The trajectories terminate above the dashed line, where $a_1(1 + e_1) = a_2(1 - e_2)$ and the planets would collide at conjunction.

libration centers at $\theta_1 = 180°$ and $\theta_2 = 0°$ and retrograde orbital precessions. Along the sequence for a given m_1/m_2, the fractional distance between the planets at conjunction, $(a_1/a_2)(1 + e_1) - (1 - e_2)$, decreases with decreasing e_2, and the system becomes unstable at a point above the dashed line in Figure 14, where $a_1(1 + e_1) = a_2(1 - e_2)$ and the planets would collide at conjunction. We can see from Figure 14 that the configurations with $\theta_1 \approx 180°$ and $\theta_2 \approx 0°$ tend to a sequence with $e_1 = 0$ and e_2 above 0.37 in the limit $m_1/m_2 \rightarrow \infty$. These are the pericentric libration configurations found by Beaugé (1994) for the exterior 2:1 resonance in the planar, circular, restricted three-body problem.

4.3. *Effects of Total Planetary Mass*

We consider in this subsection the effects of a larger total planetary mass on the stability of the resonance configurations found in §§ 4.1 and 4.2 for $(m_1 + m_2)/m_0 = 10^{-3}$. We have used the configurations indicated by the dashed lines in Figure 7 as initial conditions for calculations in which $m_1 + m_2$ is increased at a rate of $d \ln(m_1 + m_2)/dt = 10^{-6}/P_{2,0}$ while m_1/m_2 is kept constant. These configurations with $m_1/m_2 = 1$, 0.3, and 0.1 become unstable when $(m_1 + m_2)/m_0$ exceeds 0.0037, 0.0041, and 0.0043, respectively. Similar calculations with the configurations indicated by the dashed lines in Figure 8 with $m_1/m_2 = 3$, 5, and 10 as initial conditions show that these configurations are stable for $(m_1 + m_2)/m_0$ up to at least 10^{-2}.

For the antisymmetric configurations with $\theta_1 \approx 180°$ and $\theta_2 \approx 0°$, the minimum e_2 (and the minimum fractional distance between the planets at conjunction) at which the configurations become unstable increases with increasing total planetary mass. We have used the configurations at the top of the trajectories shown in Figure 14 with $e_2 \approx 0.7$ and $m_1/m_2 = 0.1$, 1, and 10 as initial conditions for calculations in which $m_1 + m_2$ is increased, and they remain stable to the end of the calculations when $(m_1 + m_2)/m_0 = 10^{-2}$. When we use instead the configurations indicated by the triangles in Figure 14 as initial conditions, the cases with $m_1/m_2 = 0.1$ and 1 are stable for $(m_1 + m_2)/m_0$ up to at least 10^{-2}, but the case with $m_1/m_2 = 10$ becomes unstable when $(m_1 + m_2)/m_0$ exceeds 0.0096.

It is likely that many (if not all) of the asymmetric configurations shown in Figure 9 for $m_1/m_2 = 0.3$ (which is close to $m_1/m_2 = 0.32$ of the GJ 876 planets) are unstable for the total mass of the GJ 876 planets [$(m_1 + m_2)/m_0 = 0.0095$], because the configuration at $t = 0$ is the $m_1/m_2 = 0.3$ configuration from Figure 7 examined above and it is unstable for $(m_1 + m_2)/m_0 > 0.0041$. Thus, for a system with masses like those in GJ 876, there are stable 2:1 resonance configurations with $(\theta_1, \theta_2) \approx (180°, 0°)$, in addition to those with $(\theta_1, \theta_2) \approx (0°, 180°)$ and $(0°, 0°)$ that can be obtained from differential migration of planets with constant masses. However, the planets are sufficiently massive that asymmetric configurations like those in Figure 9 are probably unstable.

5. DISCUSSION AND CONCLUSIONS

We have shown that there is a diversity of 2:1 resonance configurations for planar two-planet systems. We began with a series of differential migration calculations, with planets having constant masses and initially circular orbits, and found the following types of stable 2:1 resonance configurations: (1) antisymmetric configurations with the mean-motion resonance variables $\theta_1 = \lambda_1 - 2\lambda_2 + \varpi_1$ and $\theta_2 = \lambda_1 - 2\lambda_2 + \varpi_2$ librating about 0° and 180°, respectively (as in the Io-Europa pair); (2) symmetric configurations with both θ_1 and θ_2 librating about 0° (as in the GJ 876 system); and (3) asymmetric configurations with θ_1 and θ_2 librating about angles far from either 0° or 180°. Systems with $m_1/m_2 \lesssim 0.95$, $0.95 \lesssim m_1/m_2 \lesssim 2.55$, $2.55 \lesssim m_1/m_2 \lesssim 2.75$, and $m_1/m_2 \gtrsim 2.75$ show different types of evolution (Table 1), and their trajectories in the e_1-e_2 plane are clearly distinguished (Fig. 5). The basic trajectories depend only on m_1/m_2, but the libration amplitudes and the point at which a sequence becomes unstable can be sensitive to the migration rate and the total planetary mass. Where a system is left along a sequence depends on the magnitude of the eccentricity damping or the timing of the termination of migration due to nebula dispersal. There are also stable 2:1 resonance configurations with symmetric ($\theta_1 \approx \theta_2 \approx 0°$), asymmetric, and antisymmetric ($\theta_1 \approx 180°$ and $\theta_2 \approx 0°$) librations that cannot be reached by differential migration of planets with constant masses and initially nearly circular orbits. We have analyzed the properties of the resonance configurations found in our study. The asymmetric configurations with large e_2 and the $\theta_1 \approx 180°$ and $\theta_2 \approx 0°$ configurations have intersecting orbits, while the $\theta_1 \approx \theta_2 \approx 0°$ configurations with $e_1 > 0.714$ have prograde orbital precessions. Figures 5, 11, and 14 can be used to determine whether an observed system could be near a 2:1 resonance configuration with both θ_1 and θ_2 librating.

We now describe several mechanisms by which the resonance configurations summarized in Figures 11 and 14 can be reached. Since we found the symmetric and asymmetric configurations in § 4.1 (Fig. 11) by a combination of calculations in which m_1/m_2 is changed and differential migration calculations, they can be reached by differential migration if the planets continue to grow at different rates and m_1/m_2 changes during migration. In particular, if $m_1/m_2 \lesssim 2.75$ when the system is first captured into resonance and m_1/m_2

increases above 2.75 when $e_1 \gtrsim 0.17$, the system should cross over to the configurations with $m_1/m_2 \gtrsim 2.75$ in Figure 11. Similarly, if $m_1/m_2 \gtrsim 2.75$ when the system is first captured into resonance and m_1/m_2 decreases below 2.75 when $e_2 \gtrsim 0.49$, the system should cross over to the configurations with $m_1/m_2 \lesssim 2.75$ in Figure 11. After the planets open gaps about their orbits and clear the disk material between them, they can continue to grow by accreting gas flowing across their orbits from the inner and outer disks. If the inner disk is depleted, the situation with the outer planet growing faster and a decreasing m_1/m_2 may be more likely (Kley 2000).

A mechanism by which the $\theta_1 \approx 180^\circ$ and $\theta_2 \approx 0^\circ$ configuration in § 4.2 (Fig. 14) can be reached is a migration scenario involving inclination resonances. Thommes & Lissauer (2003) have studied the capture into and evolution in 2:1 resonances due to differential migration for orbits with small initial inclinations. For the case with $m_1/m_2 = 1$, the system is initially captured into eccentricity-type mean-motion resonances only (with both θ_1 and θ_2 librating), and the initial evolution after capture is similar to that of the planar system discussed in § 3. But when e_1 grows to $\sim$0.6, the system also enters into inclination-type mean-motion resonances (with both $2\lambda_1 - 4\lambda_2 + 2\Omega_1$ and $2\lambda_1 - 4\lambda_2 + 2\Omega_2$ librating, where $\Omega_{1,2}$ are the longitudes of ascending node), and the orbital inclinations begin to grow. The system eventually evolves out of the inclination resonances, and interestingly, the eccentricity resonances switch from the $\theta_1 \approx \theta_2 \approx 0^\circ$ configuration to the $\theta_1 \approx 180^\circ$ and $\theta_2 \approx 0^\circ$ configuration at the same time. Thommes & Lissauer (2003) have noted that the inclination resonances are not encountered until e_1 grows to $\sim$0.6, which requires m_1/m_2 to be less than about 2 for planets with constant masses. From the results in § 3 (Fig. 5*a*), we find that the boundary in m_1/m_2 for e_1 to reach $\sim$0.6 is more precisely $m_1/m_2 \lesssim 2.75$. However, if we allow m_1/m_2 to change during migration, as described in the previous paragraph, it would be possible for e_1 to grow to $\sim$0.6 even for systems with final $m_1/m_2 \gtrsim 2.75$ (see Fig. 11). Thus, it may be possible to reach the $\theta_1 \approx 180^\circ$ and $\theta_2 \approx 0^\circ$ configuration by evolving through inclination resonances for non-coplanar systems with a wide range of final m_1/m_2.

Finally, there is a mechanism for establishing mean-motion resonances in planetary systems that does not involve migration due to planet-disk interaction. Levison et al. (1998) have found that a significant fraction of systems at the end of a series of simulations starting with a large number of planetary embryos have mean-motion resonances. More recently, Adams & Laughlin (2003) have performed a series of *N*-body simulations of crowded planetary systems with 10 giant planets initially in the radial range 5 AU $\leq a \leq$ 30 AU. After 10^6 yr, there are often only two or three planets remaining in a system, and a surprisingly large fraction ($\sim$10%) of the systems have a pair of planets near resonance (roughly equally distributed among the 2:1, 3:2, and 1:1 resonances), although not all of the resonant pairs will survive on longer timescales. If there is no additional damping mechanism, the resonance configurations produced by multiple-planet scattering in crowded planetary systems are likely to have moderate-to-large orbital eccentricities and relatively large libration amplitudes. A more detailed analysis of the resonances produced by this mechanism is needed, but there is no obvious reason to suspect that it cannot produce any of the 2:1 resonance configurations with moderate-to-large orbital eccentricities presented in §§ 3 and 4, provided that the configuration is stable for relatively large libration amplitudes.

The number of multiple-planet systems is expected to increase significantly in the next few years. Our results show that a wide variety of 2:1 resonance configurations can be expected among future discoveries and that their geometry can provide information about the origin of the resonances.

It is a pleasure to thank Stan Peale for his contributions to the early stages of this work and for many useful discussions. I also thank G. Laughlin and E. W. Thommes for informative discussions. This research was supported in part by NASA grants NAG5-11666 and NAG5-13149.

REFERENCES

Adams, F. C., & Laughlin, G. 2003, Icarus, 163, 290
Beaugé, C. 1994, Celest. Mech. Dyn. Astron., 60, 225
Beaugé, C., Ferraz-Mello, S., & Michtchenko, T. A. 2003, ApJ, 593, 1124
Beaugé, C., & Michtchenko, T. A. 2003, MNRAS, 341, 760
Bryden, G., Różyczka, M., Lin, D. N. C., & Bodenheimer, P. 2000, ApJ, 540, 1091
Duncan, M. J., Levison, H. F., & Lee, M. H. 1998, AJ, 116, 2067
Ferraz-Mello, S., Beaugé, C., & Michtchenko, T. A. 2003, Celest. Mech. Dyn. Astron., 87, 99
Goldreich, P., & Sari, R. 2003, ApJ, 585, 1024
Hadjidemetriou, J. D., & Psychoyos, D. 2003, in Galaxies and Chaos, ed. G. Contopoulos & N. Voglis (Berlin: Springer), 412
Ji, J., Kinoshita, H., Liu, L., Li, G., & Nakai, H. 2003, Celest. Mech. Dyn. Astron., 87, 113
Kley, W. 2000, MNRAS, 313, L47
Kley, W., Peitz, J., & Bryden, G. 2004, A&A, 414, 735
Laughlin, G., & Chambers, J. E. 2001, ApJ, 551, L109
Lee, M. H., & Peale, S. J. 2002, ApJ, 567, 596
Lee, M. H., & Peale, S. J. 2003a, in ASP Conf. Ser. 294, Scientific Frontiers in Research on Extrasolar Planets, ed. D. Deming & S. Seager (San Francisco: ASP), 197
———. 2003b, ApJ, 592, 1201
Levison, H. F., Lissauer, J. J., & Duncan, M. J. 1998, AJ, 116, 1998
Malhotra, R. 1999, Lunar Planet. Sci. Conf., 30, 1998
Marcy, G. W., Butler, R. P., Fischer, D. A., Laughlin, G., Vogt, S. S., Henry, G. W., & Pourbaix, D. 2002, ApJ, 581, 1375
Marcy, G. W., Butler, R. P., Fischer, D., Vogt, S. S., Lissauer, J. J., & Rivera, E. J. 2001, ApJ, 556, 296
Mayor, M., Udry, S., Naef, D., Pepe, F., Queloz, D., Santos, N. C., & Burnet, M. 2004, A&A, 415, 391
Message, P. J. 1958, AJ, 63, 443
Rivera, E. J., & Lissauer, J. J. 2001, ApJ, 558, 392
Snellgrove, M. D., Papaloizou, J. C. B., & Nelson, R. P. 2001, A&A, 374, 1092
Thommes, E. W., & Lissauer, J. J. 2003, ApJ, 597, 566
Ward, W. R. 1997, Icarus, 126, 261
Wisdom, J., & Holman, M. 1991, AJ, 102, 1528